ADVANCED INTELLIGENT SYSTEMS
Open Access
www.advintellsyst.com

# A Dual-Origami Design that Enables the Quasisequential Deployment and Bending Motion of Soft Robots and Grippers

*Woongbae Kim, Jaemin Eom, and Kyu-Jin Cho**

**Soft fluidic actuators produce continuous and life-like motions that are intrinsically safe, but current designs are not yet mature enough to enable large deployment with high force and low-cost fabrication methods. Herein, soft fluidic actuators with two superimposed origami architectures are reported. Driven by a fluid input, the presented dual-origami soft actuators produce quasisequential deployment and bending motion that is guided by unsymmetric unfolding of low-stretchable origami components. The dominance between the deployment and bending can be shifted by varying the unfolding behavior, enabling preprogramming of the motion. The proposed origami-inspired soft actuators are directly fabricated by low-cost fused deposition modeling 3D printing and subjected to heat treatment postprocessing to enhance the fluid sealing performance. Finally, soft gripper applications are presented and they successfully demonstrate gripping tasks where each requires strength, delicacy, precision, and dexterity. The dual-origami approach offers a design guidance for soft robots to embody grow-and-retract motion with a small initial form factor, promising for applications in next-generation soft robotic systems. An interactive preprint version of the article can be found here: https://www.authorea.com/doi/full/10.22541/au.163698906.68661340.**

## 1. Introduction

Advances in soft robotics have presented the way robots interact with humans or unstructured environments. In response to external stimuli, such as fluidic pressure,[1–7] electric signals,[8–10] magnetic fields,[11,12] and motor-tendon actuation,[13–15] the architected soft matters, mostly elastomers, produce continuous and adaptive motions that allow delicate handling of fragile objects or shape adjusting to unstructured environments. Utilizing the inherent features of softness, soft robots are gradually being used for safety demanding applications or near-human applications such as soft grippers,[11,13,16] soft manipulators,[3,9] mobile robots,[2,4,5,10,12,14] assistive wearable robots,[6,15] and minimally invasive surgical tools.[7,17] The established design method for soft fluidic robots is to embody anisotropic deformation in soft bodies by carving geometric patterns of extensible fluidic networks and embedding inextensible strain-limiting appendages (e.g., paper strips, fabrics, tendons).[18,19] Consequently, the applied fluid causes asymmetric extension of fluidic networks and strain-limiting appendages, and the whole soft body produces preprogrammed motion such as bending,[19–22] twisting,[23] and contraction.[24,25] Researches to date have mainly focused on architecting fluidic networks and have achieved rapid actuation,[20] high aspect ratio design,[26] and high force generation.[21,22] However, the current design method compels soft robots to be shaped as a long elastomeric beam or a cylinder because their form factors are subordinated to inextensible strain-limiting appendages, which may limit their spatial efficiency and make it inconvenient for soft fluidic robots to be used with other mechanical elements due to physical interferences.

Origami deployable architectures have unique features that are folded into compact forms when not in use and can be transformed into large shapes to be functional. This deployment combined functionality provides portability and mobility at the folded state while it can generate large motions at the deployed state. For example, in nature, flying insects such as ladybugs and earwigs fold and retract their hind wings for reduced inertia and only deploy and flap them during flight.[27,28] With additional benefits such as desired shapes or motions which can be robustly guided by kinematics, and a large variety of constituting materials (from compliant paper to steel plate), the origami design has been considered as a promising method for deployable machines with possible applications in mobile robots,[29–31] manipulators,[32,33] space missions,[34,35] and biomedical tools.[33,36] Likewise, several researches of soft fluidic robots have adopted origami deployable architectures. Martinez et al developed paper-elastomer composite soft fluidic robots including Yoshimura origami cylinder structure (so-called bellow-like

W. Kim, J. Eom, K.-J. Cho
Department of Mechanical Engineering
Seoul National University
1 Gwanak-ro, Gwanak-gu, Seoul 08826, Korea
E-mail: kjcho@snu.ac.kr

The ORCID identification number(s) for the author(s) of this article can be found under https://doi.org/10.1002/aisy.202100176.

© 2021 The Authors. Advanced Intelligent Systems published by Wiley-VCH GmbH. This is an open access article under the terms of the Creative Commons Attribution License, which permits use, distribution and reproduction in any medium, provided the original work is properly cited.

**DOI: 10.1002/aisy.202100176**

pattern) that grow or bend due to glued facets or an attached strip.[37] Li et al presented soft fluid robots in which an origami skeleton is sealed by flexible skin, and negative pressure is applied to fold the crease lines in a preprogrammed sequence.[38] Chen et al developed a hybrid actuator with a motor-driven tendon and a fluid-driven asymmetric Yoshimura origami cylinder, in which the effective length of the bending configuration can be changed.[39] These existing works successfully imported origami deployable architectures' large range of motion into fluidic networks, while they have not yet focused on designing or programming additional motions beyond kinematics of origami deployment.

Recently, implementation of soft and compliant materials widened the accessible regime of origami folding over origami kinematics.[40–42] Our previous work, "a dual-morphing stretchable origami," presented an entirely stretchable origami that deploys by unfolding and then produces additional motion by anisotropic stretching.[42] Although this dual-morphing principle that utilizes both morphing principles of unfolding and stretching could achieve extreme shape morphing, there exist several limitations originating from the essential use of highly stretchable materials: 1) low force due to incapability of holding high pressure, 2) poor reliability due to nonlinearity of materials and Mullins effect, 3) slow response time due to heavy reliance on material response speed, 4) difficulty in control due to difficulties in kinematics analysis of stretching behavior, and 5) narrow material selection with only a few specific materials (expensive silicone elastomers or high-tech 3D printing materials) available. In addition, a complex fabrication process using sacrificial molds, as well as the need for deposition of multiple materials to achieve functional motion (e.g., bending) over deployment and balloon-like bloating, significantly increases fabrication cost. These drawbacks presented challenges for practical usage of the dual-morphing principle in real-world applications, highlighting a need for a new design method of a different working principle that does not rely on stretching, broadens the range of applicable materials, and enables large deployment, high force, and low-cost/easy fabrication (the detailed comparison of the dual-morphing principle and the current work is shown in Table S1, Supporting Information).

In this article, we present a soft robot with a small initial form factor that undergoes quasisequential deployment and bending motion driven by a single fluid input, enabled by a dual-origami design in which both the fluidic network and the strain-limiting layer are compliant origami architectures. We selectively placed the folded strain-limiting layer in between the facets of the folded fluidic network, building the latter to be more extensible than the former. Accordingly, in an early stage of the response to fluid pressure, the two elements both unfold simultaneously, and the whole body mainly deploys, while slight bending also occurs simultaneously, depending on the stiffness of the origami strain-limiting layer. When the strain-limiting layer is almost fully unfolded, the fluidic network unfolds solely to drive the whole body to bend, accessing the regime outside of origami kinematics utilizing flexibility of the soft material. The motion is preprogrammable through adjusting design parameters of the origami strain-limiting layer. The finite-element analysis (FEA) and experimental results provide relationships between the quasisequential deployment and bending motion and the geometries, to select an appropriate parameter value for given desired motion. Dual-origami soft actuators can be directly printed by a low-cost fused deposition modeling (FDM) 3D printer using flexible filaments such as thermoplastic polyurethane (TPUs) or thermoplastic elastomers (TPEs), with an introduction of heat treatment post-processing for soft fluidic robots to leverage high pressure holds (>200 kPa). The proposed design can generate high force (>3 kg), the same way other low-stretchable soft fluidic robots that can hold high fluidic pressure (e.g., pouch motors, HASEL actuators).[8,43] Using dual-origami soft bending actuators as deployable fingers and integrating them with a commercial suction cup, we built a versatile soft gripper that allows the selective use of two gripping mechanisms, without spatial interference between the suction cup and the fingers. Our new design method for soft robots achieved an effective spatial extension from a limited form factor and embodies not only portability but also cooperative abilities with other mechanical elements through growth and retract.

## 2. Results

### 2.1. Design of Dual-Origami Soft Bending Actuators

A common six-module dual-origami soft fluidic bending actuator that is initially folded and deploys through dual-origami unfolding is shown in **Figure 1**A and Movie S1, Supporting Information. Two integral components of the dual-origami design are the origami fluidic network and the origami strain-limiting layer based on conventional deployable origami architectures. We selected Miura-ori polyhedron and zigzag-folded Miura-ori as the parent origami frame of two components, respectively.[44] These origami architectures have large potential deployment ratios springing from their asymmetric geometries, where the facets are serially connected via crease lines at each end, as well as additional advantages of flat foldability and rigid foldability. A single Miura-ori polyhedron module comprises four parallelogram facets connected in a closed form, and when folded, each layer contains two parallelogram facets and a diamond-shaped crease line loop (Figure 1B). A single-module zigzag-folded Miura-ori is identical to half of the Miura-ori polyhedron, which comprises two parallelograms not in a closed form (Figure 1B). For soft robotic application, we modified/determined their geometry as follows. 1) For both origami architectures, we merged two parallelograms on the same layer by removing the shared crease line because the folding of the removed crease line can be replaced by the bending of the merged flexible facet. 2) The Miura-ori polyhedron's diamond-shaped crease line loops at the top and bottom were enclosed by plates of the same shape for fluidic actuation. 3) We optionally made a V-cut at the crease lines of the zigzag-folded Miura-ori to tune the folding stiffness. As shown in Figure 1A,B, the proposed dual-origami design is in the initial folded form where the zigzag-folded Miura-ori strain-limiting layers are interposed between the facets of the Miura-ori polyhedron fluidic network.

Both origami components are built to be C-channel-shaped geometry in which their facets are serially connected in the direction of stacking via C-channel shaped crease lines. When bending moments are applied at the C-channel-shaped crease lines, bending intensively occurs as if origami unfolding occurs.


© 2021 The Authors. Advanced Intelligent Systems published by Wiley-VCH GmbH

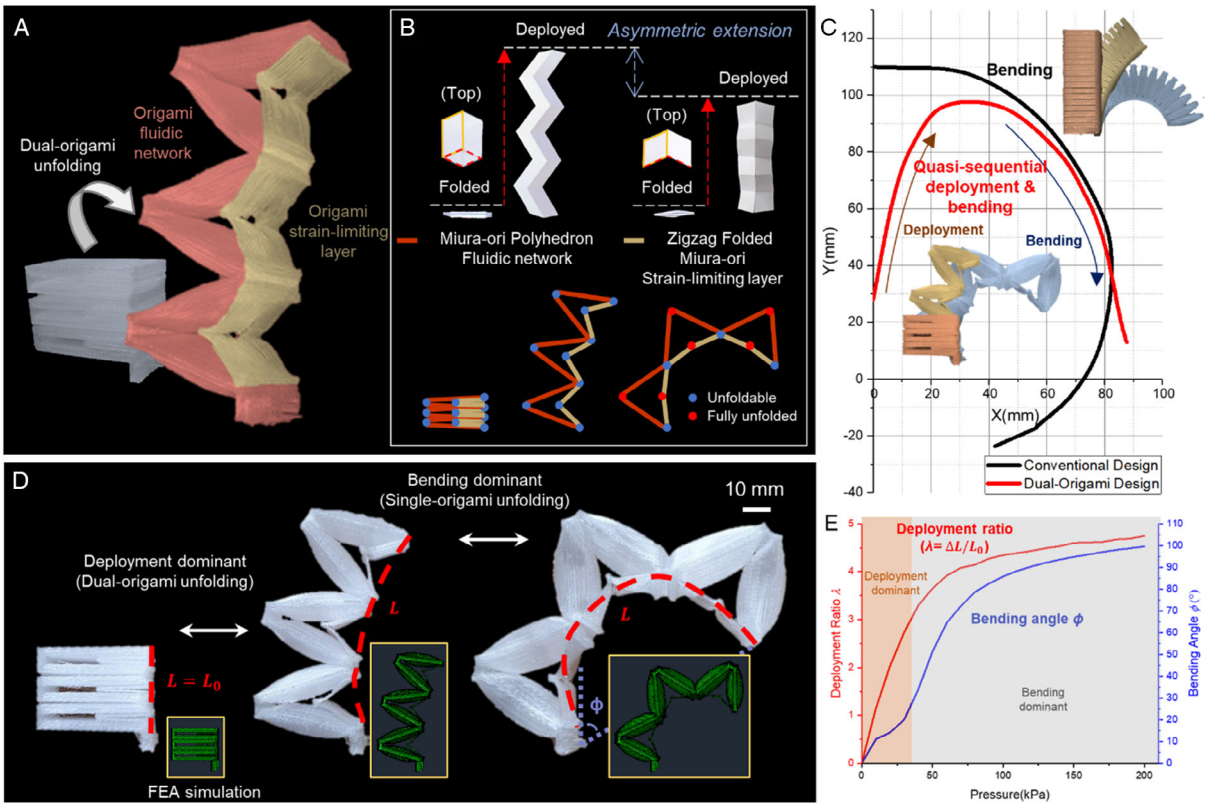


**Figure 1.** Design and principle of the dual-origami soft fluidic bending actuator. A) Unfolding of six-module dual-origami soft fluidic bending actuator. Note that the colors (red and yellow) are virtually overlaid to distinguish the components and are actually monochromatic (white). B) Parent paper origami structures and their schematic drawings of behavior in a dual-origami soft fluidic bending actuator. C) End-tip trajectories of dual-origami soft fluidic bending actuator (red) and conventional soft pneumatic bending actuator (black). D) Quasisequential deployment and bending motion of six-module dual-origami soft fluidic bending actuator. Insets represent corresponding simulation result. E) Deployment ratio ($\lambda$, red) and bending angle ($\phi$, blue) in response to applied pressure.

Because the applied fluidic pressure at the Miura-ori polyhedron fluidic network produces bending moments at entire crease lines directly (fluidic network) or indirectly (strain-limiting layer), dual-origami components unfold simultaneously. We defined a single-module dual-origami unit as the structure consisting of a flat fluidic network with two parallel facets and a strain-limiting layer of a single facet connected to it. A multimodule dual origami can be readily designed by the stacking module units and connecting them via C-channel-shaped crease lines.

The quasisequential deployment and bending behavior of a representative six-module dual-origami soft fluidic bending actuator was experimentally measured and plotted in Figure 1C (red line). This peculiar motion can be distinguished into two modes that quasisequentially appear in accordance with the applied fluid pressure level (Figure 1D). The first mode, a deployment-dominant mode, appears at relatively low fluid pressure ($P < 40$ kPa), and both the origami fluidic network and the origami strain-limiting layer unfold simultaneously. Therefore, the deployment ratio ($\lambda = \frac{(L-L_0)}{L_0}$, where $L$ is the effective layer length and $L_0$ is its initial value), in response to applied fluidic pressure, rapidly increases compared with the bending angle ($\phi$) (Figure 1E, red area). As the applied fluid pressure increases, the second mode, a bending-dominant mode appears, and the unfolding speed of the origami fluidic network overwhelms the unfolding speed of the origami strain-limiting layer. This is because the strain-limiting layer is nearly completely unfolded, yet the fluidic network is not, and thus $\phi$ surges while $\lambda$ slowly increases (Figure 1E, gray area). When the applied pressure is decreased, the deployed soft body retracts due to its own elasticity. We also built a conventional soft bending actuator (widely known as PneuNet design)[19,20,22] and plotted its behavior for comparison (Figure 1B, black line). Although the initial length $L_0$ of the dual-origami design (29.5 mm) was much lower than the $L_0$ of the conventional design (107 mm), the dual-origami actuator was unfolded similarly in scale to the conventional actuator, and the bending trajectories overlapped near $16° < \phi < 80°$ (the conventional design is still advantageous for large bending because of the trade-off relationship between deployment and bending, which is further discussed in Section 2.2). The aspect ratio of the dual-origami bending actuators was initially 0.657 and increased up to 3 when unfolded, which is similar to the conventional soft bending actuator's aspect ratio of 2.89 (dimensions of both actuators are shown in Figure S1, Supporting Information).


© 2021 The Authors. Advanced Intelligent Systems published by Wiley-VCH GmbH

### 2.2. Preprogramming of Quasisequential Deployment and Bending Motion

The bending angle of the two-module dual-origami soft fluidic bending actuator is geometrically derived as $\phi \approx (\theta_{free} - \theta_{ori})$ and the change in effective layer length can be written as $\Delta L \approx 2\theta_{ori} l_{network}$ (See Figure S2 and Supporting Information for details on the simplified kinematic model. Variables are defined in **Figure 2**A. $\theta_{ori}$ and $\theta_{free}$ are the angles between the two-module dual-origami soft fluidic bending actuators with an attached and unattached origami strain-limiting layer, respectively. $l_{layer}$ and $l_{network}$ are side lengths of the origami layer and the fluidic network, respectively. The ratio of the bending angle to the deployment ratio can be derived as $\frac{\phi}{\lambda} = \frac{\phi}{\Delta L/L_0} = \frac{L_0}{2l_{network}}\left(\frac{\theta_{free}}{\theta_{ori}} - 1\right)$ or $\frac{\phi}{\lambda} = CA_0$, where $A_0 = \frac{L_0}{l_{network}}$ is an initial aspect ratio and $C = \frac{1}{2}\left(\frac{\theta_{free}}{\theta_{ori}} - 1\right)$. We named $C$ as the bending-to-deployment ratio factor because it represents the dominance of bending to deployment during the quasisequential deployment and bending motion. A high value of $C$ means that the dominance of bending is large; when the robot only bends without deployment, $C \to \infty$ (e.g., when the inextensible strain-limiting layer is attached, like conventional soft bending robots) and when the robot only deploys without bending, $C = 0$ (e.g., origami fluidic network without a strain-limiting layer). For common dual-origami soft fluidic bending actuators, it was observed that $C$ rapidly increases at the transition pressure at which the dominance shift occurs (Figure 2B).

In order to better understand the quasisequential deployment and bending motion, we investigated the relationship between the geometric parameters of the origami strain-limiting layer and $\theta_{ori}$ or $\theta_{free}$ by performing experiments and FEA simulations (Figure 2B-E). A crease line width of one side ($w$) and a ratio between $l_{layer}$ and $l_{network}$ ($\Lambda = l_{layer}/l_{network}$) were considered as the important geometric parameters because it was expected that the rotational stiffness of the crease line would increase with increasing $w$ and the maximum value of $\theta_{ori}$ would be geometrically determined by $\Lambda$ (Figure 2A). In both the experiment and simulation, the response of $\theta_{free}$ to applied fluid pressure was constant even though geometric parameters of the origami layer at the nearby modules were changed (Figure 2C). In contrast, the response of $\theta_{ori}$ to applied fluid pressure was affected by $w$ and $\Lambda$. It was noteworthy that the change in $w$ gradually shifts the response while $\Lambda$ changes it significantly (Figure 2D,E). For example, the increase in $w$ from 3 to 12 mm decreased $\theta_{ori}$ from 58.16° to 49.56° at 100 kPa (Figure 2D, for $\Lambda = 0.476$), and the increase in $\Lambda$ from 0.238 to 0.476 increased $\theta_{ori}$ from 25.47° to 54.43° at 100 kPa (Figure 2E, for $w = 6$ mm). The result also indicates that the amount of deployment and bending should be selectively preprogrammed with consideration of their tradeoff relationship; $\phi$ decreases as $\theta_{ori}$ increases but $\lambda$ is proportional to $\theta_{ori}$. Accordingly, $C$ was 0.158 at 20 kPa for the most deployable case, while $C$ was 0.825 at 20 kPa for the most bendable case, which is about 5.22 times difference (Figure 2B).

To confirm the preprogrammability of the quasisequential deployment and bending motion, six-module dual-origami soft fluidic bending actuators with different geometric parameters were built (Figure 2F-M). As shown in Figure 2F,J, Movie S2, and S3, Supporting Information, we could design clear differences in motion determined by $w$ and $\Lambda$; their end-tip trajectories are plotted in Figure 2G,K, respectively. $\lambda$ decreased from 4.78 to 4.32 and $\phi$ increased from 90.9° to 106.9° as $w$ increased from 3 to 12 mm, whereas increase in $\Lambda$ from 0.238 to 0.476 greatly increased $\lambda$ from 2.35 to 4.75 and decreased $\phi$ from 144.75° to 99.66° (at $P = 200$ kPa, Figure 2H,I,L,M). The result confirms that the quasisequential deployment and bending motion is more sensitive to $\Lambda$ than $w$. Therefore, it would be recommended to determine $\Lambda$ for coarse adjusting in precedence to $w$ for fine adjusting. In addition, thickness of the strain-limiting layer ($t$) can be considered for preprogramming of the motion. However, it should be noted that a small change in $t$ would change motion dramatically because the bending stiffness of the layer is proportional to $t^3$, and therefore it is not recommended to tune $t$ for motion preprogramming. (Figure S3, Supporting information, shows simulation result that small change from $t = 0.6$ to 0.8 mm increases $\alpha$ significantly from 0.115 to 0.296 at 18 kPa).

### 2.3. Development of Multipurpose Soft Gripper

Soft grippers with soft fluidic bending actuators acting as fingers have emerged as a promising technology for safe and delicate pick and place including foods, pharmaceuticals, and logistics applications.[45] With conventional soft grippers, however, the object size that can be gripped is limited by the initial configuration (**Figure 3**A). To widen the gripper opening, prestressed or bidirectional soft fluidic actuators were developed,[46,47] but the problem where the grippers should only approach the object vertically to avoid collisions still remains, which may reduce the work efficiency and increase the burden of the manipulator control and operation.

We constructed a dual-origami two-finger gripping unit where each finger at both sides is a six-module dual-origami fluidic soft fluidic bending actuator. The initial configuration was designed to be parallel to the objects to achieve a wide gripper opening (Figure 3B). The total width of the two-finger unit was relatively small compared with the conventional soft robotic finger, but the finger unit could grip larger objects, even objects larger than its initial size. In addition, because the compactness greatly reduced the risk of collision, the finger unit could approach to objects via various paths (vertical, horizontal, and diagonal from bottom to top, Figure 3C).

The motion and closed configuration were preprogrammed via FEA simulation and prototyping for fast and versatile grip. When all strain-limiting layers were built with the same parameters that prefer deployment over bending (Design II of Figure 3D), the closed configuration was achieved at 100 kPa with a 93 mm gap. In addition, when the modules at the bottom were designed to be bent greatly (Design I of Figure 3D), the gripping unit formed a narrow-closed configuration with a 65 mm gap at 40 kPa. Therefore, Design I can be considered as the suitable unit that allows for fast grip with sufficient contact area during power grip (grip that wraps around an object).

The gripping force of Design I gripping unit was measured (the experimental setup is shown in Figure S4, Supporting Information, and explained in the Experimental Section). We


© 2021 The Authors. Advanced Intelligent Systems published by Wiley-VCH GmbH

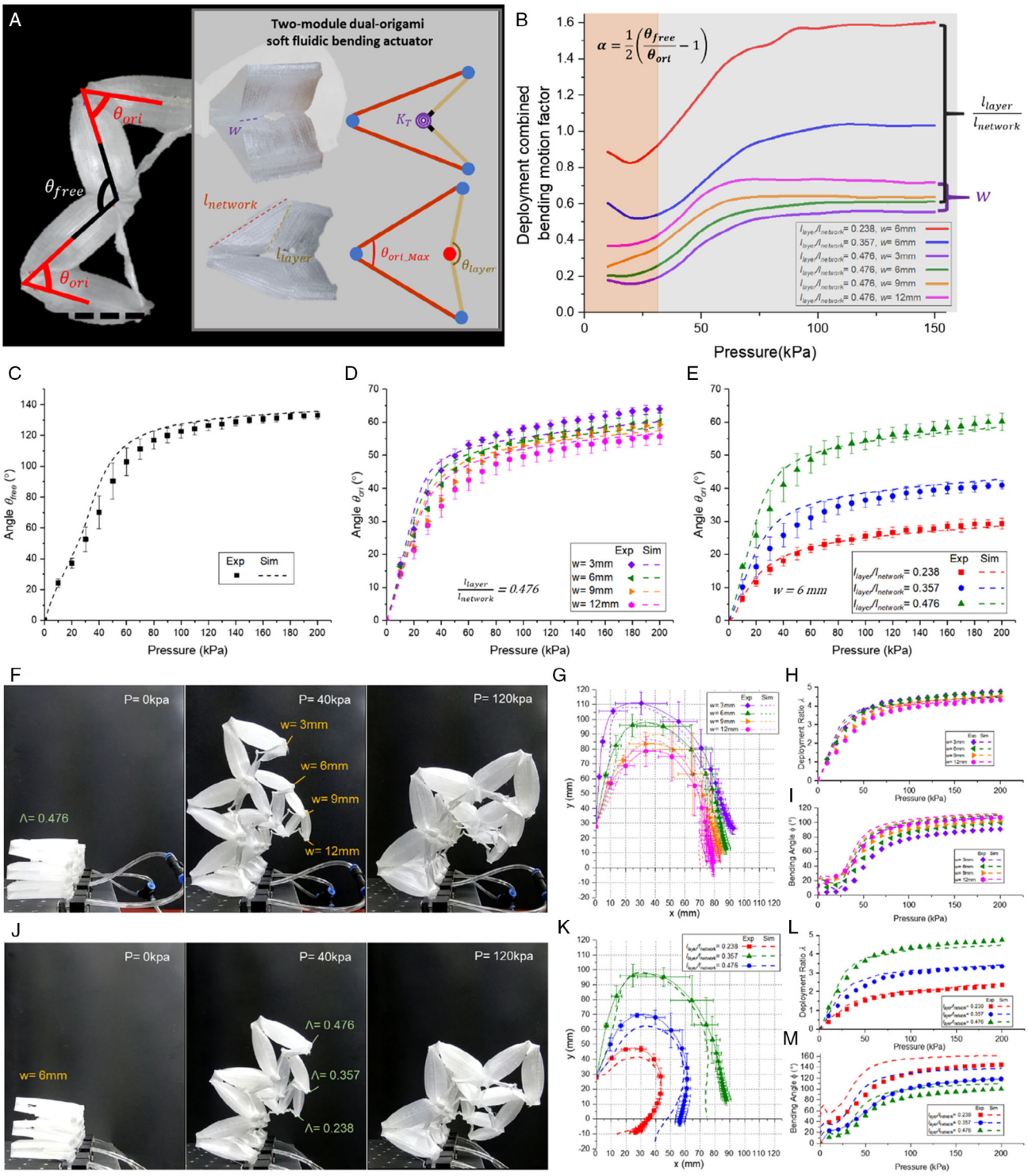


**Figure 2.** Parametric study of two-module dual-origami soft fluidic bending actuator and preprogramming of the quasisequential deployment and bending motion for six-module dual-origami soft fluidic bending actuators. A) Geometric parameters ($l/L$ and $w$) and output angles ($\theta_{ori}$ and $\theta_{free}$). B) Bending-to-deployment ratio factor ($C = \frac{1}{2}\left(\frac{\theta_{free}}{\theta_{ori}} - 1\right)$) in response to applied pressure. C) Experimental and simulation results of the angle between two modules in response to applied pressure without a strain-limiting layer and D and E) with strain-limiting layers of different D) length ratios and E) widths. F) For strain-limiting layer with different widths ($w$), six-module dual-origami soft fluidic bending actuators were placed in raw and actuated simultaneously by same applied pressure. Experimental and simulation results for G) end-tip trajectories, H) deployment ratio ($\lambda$), and I) bending angle ($\phi$) were plotted. J, K, L, and M) Same procedure as (F–I) were performed for strain-limiting layer with different length ratios ($\Lambda$).


© 2021 The Authors. Advanced Intelligent Systems published by Wiley-VCH GmbH

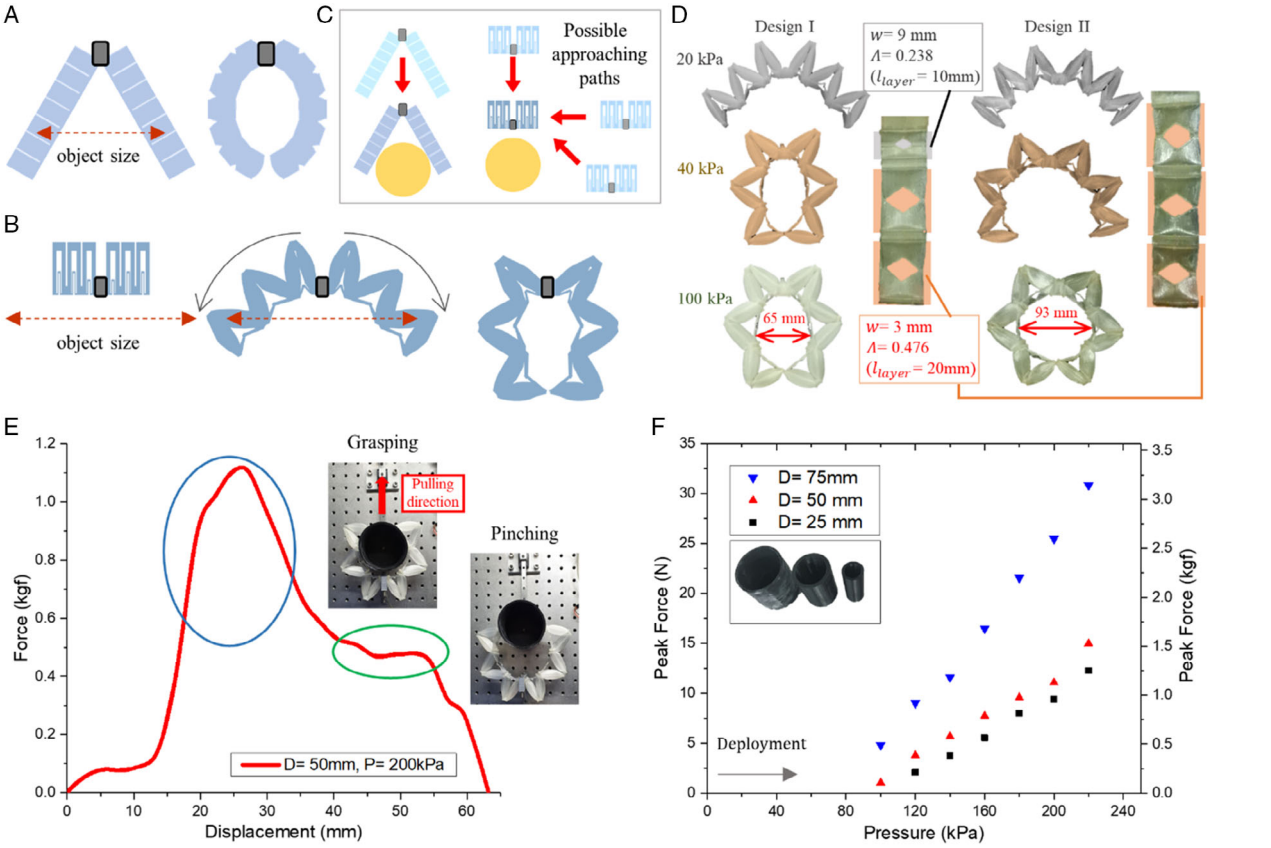


**Figure 3.** A dual-origami two-finger gripping unit. Gripping motion and affordable object size of A) a conventional soft gripper and B) a dual-origami two-finger gripping unit and comparison of their C) possible approaching paths. D) Motion and configuration design of the gripping units. E) The gripping force of the design I gripping unit ($P = 200$ kPa) when the gripped cylinder ($D = 50$ mm) is pulled out. F) Peak gripping forces of the Design I gripping unit in response to applied pressure for different cylinder diameters.

tested gripping three poly lactic acid cylinders of different diameters, 25, 50, and 75 mm. While the gripping unit held the cylinders, the cylinders were pulled at a uniform speed (3.3 mm $s^{-1}$). As shown in **Figure 4**E, the peak force appeared during power grip, and then a relatively uniform force was measured during pinch grip, and finally the cylinder was completed pulled out. At 220 kPa, the peak forces of 3.15, 1.53, and 1.25 kgf were measured for 75, 50, and 25 mm cylinders, respectively (Figure 3F). The gripping unit is lightweight (56.8 g), and the payload-to-weight ratio exceeds 55. We also tested for repeatability of the gripping unit. After 1000 cycles at 40 kPa, the bending angle of the gripping unit was changed by 8.19% compared with the 200 cycles (Figure S5, Supporting information).

As an application that leverages the spatial benefit of the retractable finger gripping unit, we developed a versatile soft gripper that uses both dual-origami fingers and suction gripper (VSS40-S-X, F.TEC, Figure 4A). For conventional grippers that complementarily utilize the advantages of finger grip and suction grip (in order to grip from rough and rounded object to flat and smooth object), protruding fingers interfere with the suction gripper when contacting the objects, and this problem required additional actuators and control strategies, for example, attaching linear actuator to suction gripper.[48] In the case of our proposed versatile gripper, the folded fingers are at the rear of the suction cup; they inherently do not interfere with the suction gripper. When the finger units are actuated, they deploy to the front of the suction gripper and can grip the object by themselves or even collaborate with the suction gripper. We attached the versatile gripper to a conventional robotic arm (M1013, Doosan Robotics) and conducted a pick-and-place task for ten objects (Figure 4B and Movie S4, Supporting Information). The soft fingers could grip various objects ranging from soft and light objects (e.g., 6-g mask, soft doll, confectionery) to a 2.5-kg dumbbell (Figure 4C). The suction grip was selectively used for flat objects, and fingers could be sequentially used for collaborative grasping (soup bowl). Moreover, by attaching artificial nails at the tip, the fingers could pick up a flat coin, reorient it in the upright position, and insert it in a slot precisely (Movie S5, Supporting Information, and Experimental section for details; tasks that each requires strength, delicacy, precision, and dexterity were conducted).

The preprogrammability of the motion also enables customizing the dual-origami two-finger gripping unit according to the object shape. As shown in **Figure 5**A, we built a two-finger gripping unit customized for box-shaped objects. Two stain-limiting layers at the bottom and middle modules were


© 2021 The Authors. Advanced Intelligent Systems published by Wiley-VCH GmbH

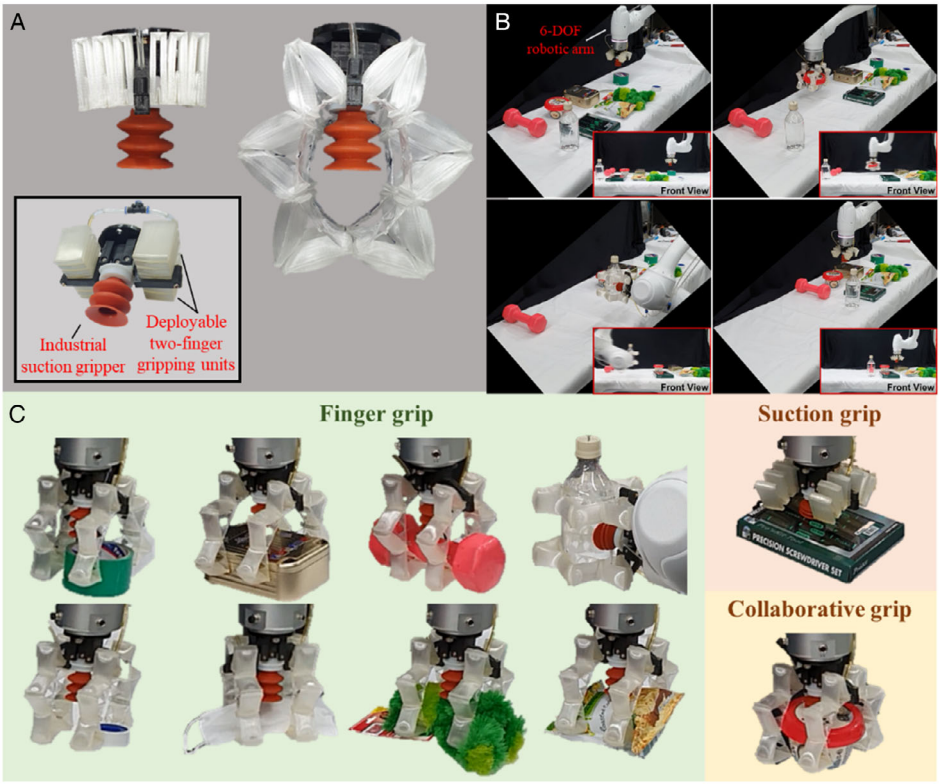


**Figure 4.** A versatile soft gripper. A) Overview of the developed gripper. B) Pick and place for various objects of irregular shapes and sizes. C) Depending on the object and environment, finger grip (green), suction grip (red), and collaborative grip (yellow) could be considered respectively.

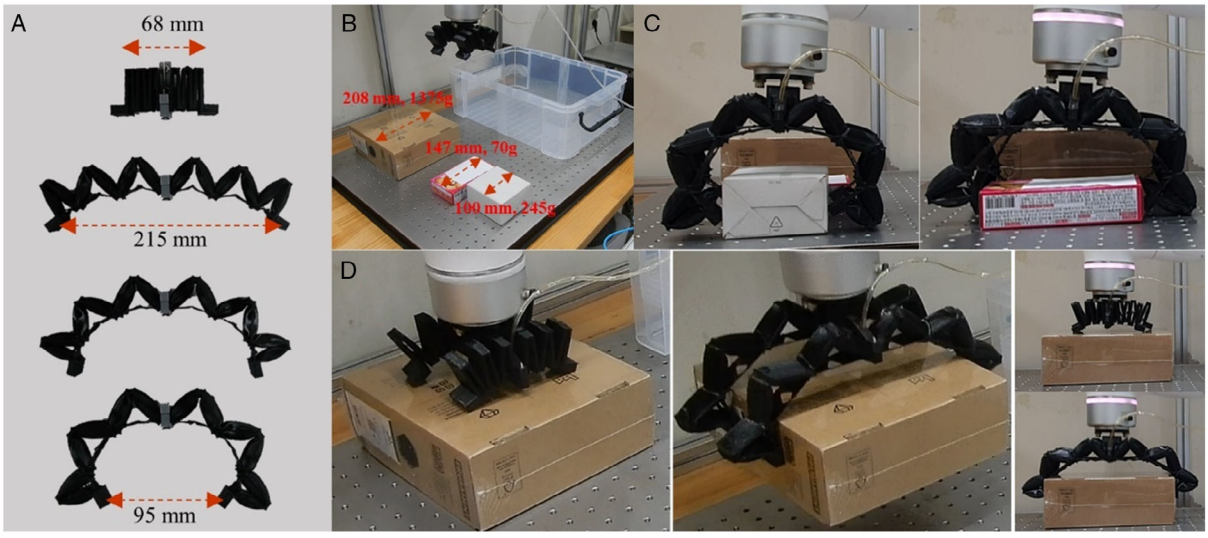


**Figure 5.** A soft gripper customized for box-shaped objects. A) Overview of the two-finger gripping unit for box-shaped objects. B) Box-shaped objects of different sizes. C,D) Soft gripper picking and placing different boxes (Movie S6, Supporting Information).

designed to be long ($\Lambda = 0.531$, $w = 6$ mm), while the strain-limiting layer at the top module was designed to be short ($\Lambda = 0.231$, $w = 9$ mm). Consequently, the two-finger gripping unit undergoes two-step motion of first widening the gripper opening significantly (from 68 to 215 mm) and then closing it moderately (Figure 5A). In the demonstration of the soft gripper with the developed two-finger gripping units, the box-shaped objects with different sizes (width of 100−208 mm, Figure 5B) were picked and placed (Figure 5C,D, and Movie S6, Supporting Information).


© 2021 The Authors. Advanced Intelligent Systems published by Wiley-VCH GmbH

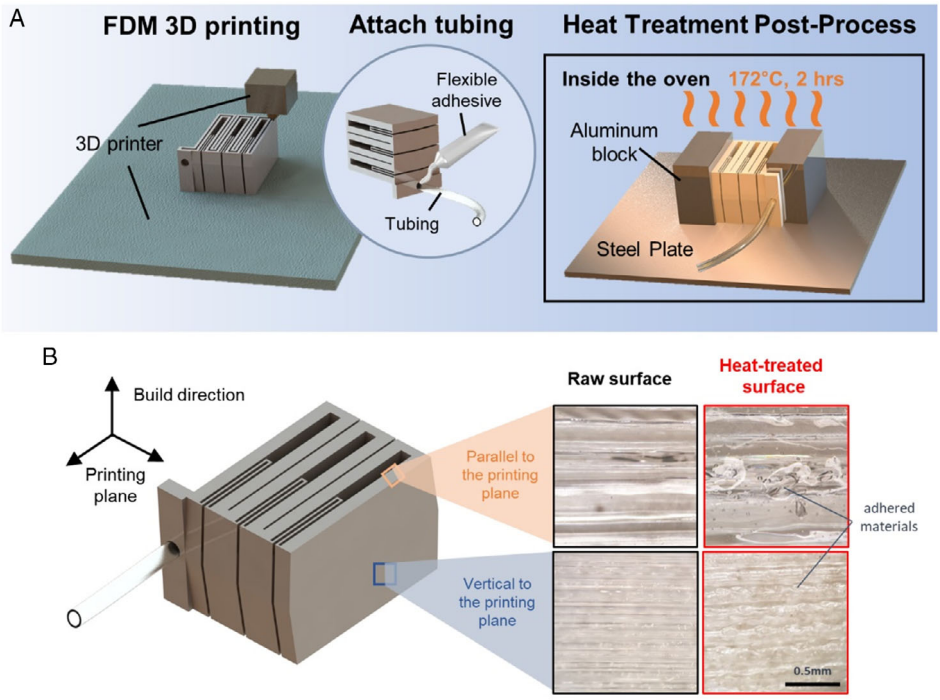


**Figure 6.** Fabrication and reinforcement of the dual-origami soft fluidic bending actuator. A) Three-step process of fabrication. Oven heat treatment postprocess can be considered as optional if high force of the actuator is not required. B) Micrographs of raw surface and heat-treated surface.

### 2.4. 3D printing and Heat Treatment of Dual-Origami Soft Fluidic Bending Actuator

Soft fluidic robots are principally fabricated through molding and casting of elastomers.[1,18,19] However, the inevitable process of detaching cured elastomer from the molds has led to difficulties in designing complex fluidic networks because the molds are usually buried within the elastomeric structure. As a solution, using sacrificial molds, made of soluble or low-melting materials such as polyvinyl alcohol (PVA) and wax, was proposed.[49] In our previous study,[42] we have fabricated zigzag-folded shaped origami architectures by the layer stacking method using PVA molds. However, these fabrication processes are complicated and time-consuming, while requiring experienced hands due to low material stiffnesses of the sacrificial molds. Meanwhile, 3D printing has been recently studied as an automotive fabrication method for soft robots.[18,22,47,50,51] In particular, FDM is a prominent and popular open-source technology with economic merits of low initial and maintenance costs. The final products can be built without supports by bridging gaps within a few centimeters, and in recent studies, researchers have directly fabricated conventional soft bending actuators made with commercially available TPU filaments.[22,47] However, because FDM printers directly add molten material line by line, defects and gaps often occur at the boundary lines, leading to failure or fluid leakage at high fluid pressure.

We fabricated a dual-origami soft fluidic bending actuator using an FDM 3 printer, as shown in **Figure 6**A. The printed actuator can be actuated immediately after gluing a urethane tubing with an adhesive, but failure or leakage occasionally happened when high pressure (>200 kPa) was applied. For robust fabrication, we attempted heat treatment of the fluidic soft actuator in an oven, expecting leakage prevention and enhancement of pressure holding. It was important to heat using the appropriate temperature and time, 1) when either of them was insufficient, the post-processing was of little avail and 2) when the conditions were excessive, the processed product was deformed or even melted and collapsed (Figure S6, Supporting Information). During the process, the soft bending actuator was placed between aluminum blocks to prevent possible deformation of modules at both ends. The postprocessing was successful at 172 °C for 2 h (for reference, melting temperature of TPUs, $T_m$>190 °C), and the white or transparent TPUs turned yellowish after post-processing. As shown in Figure 5B, it was observed that the boundaries between printed lines became blurred and were filled with adhered materials regardless of build direction. We verified the effectiveness by printing small test pouches and comparing maximum sealing pressure for raw and heat-treated pouches. As a result, the raw pouches could withstand 129 kPa on average, while the heat-treated pouches could withstand 756 kPa on average, which is an increase of 5.58 times (Figure S7, Supporting Information).

## 3. Conclusion

In this article, we have presented a soft fluidic bending actuator that undergoes characteristic quasisequential deployment and bending motion, attributed by an asymmetric extension of dual-origami components, a folded fluidic chamber and a folded strain-limiting layer. The proposed design embodies spatial


© 2021 The Authors. Advanced Intelligent Systems published by Wiley-VCH GmbH

benefits of deployment and retraction that originate from origami architectures, as well as inherent adaptiveness of soft fluidic robots. The dual-origami soft fluidic bending actuators can be directly and automatically fabricated through accessible 3D printing technology, and additional heat treatment postprocessing was introduced to reinforce the material adhesion. Furthermore, we have investigated the kinematic features of the flexible soft origami robot and established a bending-to-deployment ratio factor to quantify the dominance shifting from deployment to bending. The relationship between design parameters and the motion was also explored and the tradeoff relationship between deployment and bending was demonstrated through preprogramming of six-module dual-origami fluidic bending actuators. Moreover, we built the deployable two-finger gripping unit that can generate high holding force (≈3.15 kg, weight 56.8 g) and applied them into a versatile soft gripper that cooperates with a commercial suction gripper. The demonstration has successfully shown that the deployable finger units can not only grow and adapt to various objects, but also can make place to the suction cup for efficient use of the entire system.

We believe that our approach provides a new design guidance of soft fluidic robots to embody the grow-and-retract motion with a small initial form factor that considers space usage, differentiating from conventional design methods that primarily focus on motion generation. In addition, the proposed design principle is implemented by nonstretchable and flexible materials, allowing wide range of material choice compared with our previous work using stretchable materials.[5–7] Future work may include fabrication using light and thin materials such as thermoplastic sheets (e.g., polypropylene, polyethylene), composite fabrics, and papers, to improve scalability and functionality. Further improvement such as sensor integration, real-time control, and analytical modeling would complement the complexity of the combined motion of deployment and bending. We expect that the unique property of a small form factor soft robot with grow-and-retract motion would be considered as a powerful option for applications in next-generation soft robotic systems, including portable or mobile application, medical devices, wearable robots, and integrated robotic systems.

## 4. Experimental Section

*3D Printing Process*: Commercially available flexible filament eFlex (TPU, shore hardness 87A, eSUN) was used as the 3D printing material, and all experiments were conducted with robots made of this material. Other flexible materials including eTPU-95A (TPU, shore hardness 95A, eSUN), NinjaFlex (TPU, shore hardness 85A, NinjaTek), and eLastic (TPE, shore hardness 85A, eSUN) were also tested and it was confirmed that all of the tested materials can be used. Open-source slicing software Ultimaker Cura (Ultimaker BV) was used to prepare stereolithography (STL) files and they were imported into DIY 3D printer CORE 200 (Making Tool) using a 0.4 mm nozzle. For stable printing, the print speed was set as slow as 20 mm $s^{-1}$, and it took about 4 h to print the six-module dual origami and about 9 h to print the dual-origami two-finger gripping unit. For stiffer material eTPU-95A, 40 mm $s^{-1}$ of print speed could be applied, and the printing time was halved. Printer performance affected the consistency of soft robots' motion because a small error in strain-limiting layer thickness (related to bending stiffness $\approx t^3$) significantly changed the dominance of deployment and bending.

*Characterization and Measurement*: For the parametric study, we prepared five six-module dual-origami soft fluidic bending actuators for each geometric parameter. Red or blue dots were marked with a pen on the side edges of the modules. A protruded diamond-shaped crease line loop at the bottom was surrounded and held by 3D-printed rigid parts, and then these rigid parts were fixed to an aluminum optical breadboard. Dual-origami soft fluidic bending actuators were installed vertically to the gravity direction to ensure that gravity did not affect the deployment. For every specimen, photographs were taken for applied pressure from 0 to 200 kPa with 10 kPa increments, which was precisely controlled by a pressure regulator (RVUM, PISCO). The photographs were analyzed with MATLAB (MathWorks). The center positions of the marked circles were automatically found and characterized based on the color information. The angle between adjacent modules ($\theta_{ori}$ and $\theta_{free}$) was derived by calculating the angle between straight lines' connecting points, and effective layer length ($L$) was derived using cubic Hermite spline of points at strain-limiting layer side. The bending angle ($\phi$)was derived by calculating the angle between the axis in the height direction and the line connecting the floor and the end-tip trajectory. For the gripping force measurement, a regulated constant pressure (from 100 to 220 kPa with 20 kPa increment for each experiments) was applied to the two-finger gripping unit, holding a cylinder located at the end of the rail connected to a load cell (333FDX, KTOYO) and a linear actuator (P16-P, Actuonix Motion Devices, Inc.). To estimate the scale of friction, the rail without external gripping force was also pulled and the friction force was measured to be as low as below 50 gf.

*Finite Element Analysis*: FEA was conducted using FEA software ABAQUS (Dassault systems). Uniaxial tensile test for eFlex was performed following iso standard ASTM D412, and the result was imported into ABAQUS as a material property. All simulation conditions were set identical to the experimental conditions; the protruded diamond shaped crease line was set as a fixed boundary condition, and the contacts between facets were considered using the "general contact condition." Nodes corresponding to the points marked in the actual experiment were selected and their unique nodal displacements were collected to calculate the angle between adjacent modules, deployment ratio, and bending angle.

*Gripping Tasks*: Movie S5 shows the soft gripper successfully conducting gripping tasks designated at the manipulation competition of Robosoft 2021. The first task requires strength to grip a heavy and large fruit (1–2 kg), and the second task requires delicacy to grip a small sized delicate fruit. Korean radish weighing 1.3 kg and raspberry were chosen respectively. The third and fourth tasks were to pick a coin an insert it into a coin slot, requiring precision and dexterity respectively. The Korean 100-won coin (24 mm diameter) was chosen and the coin slot was fabricated as 4 mm × 27 mm using an acrylic plate.

## Supporting Information

Supporting Information is available from the Wiley Online Library or from the author.

## Acknowledgements

This work was supported by the National Research Foundation of Korea (NRF) (NRF-2016R1A5A1938472) and the Technology Innovation Program (20008908) funded by the Ministry of Trade, Industry & Energy (MOTIE, Korea).

## Conflict of Interest

The authors declare no conflict of interest.

## Data Availability Statement

Research data are not shared.


© 2021 The Authors. Advanced Intelligent Systems published by Wiley-VCH GmbH

## Keywords

artificial muscles, deployable robots, origami, soft grippers, soft robotics

Received: October 29, 2021
Published online:

[1] A. D. Marchese, R. K. Katzschmann, D. Rus, *Soft Rob.* **2015**, *2*, 7.
[2] N. S. Usevitch, Z. M. Hammond, M. Schwager, A. M. Okamura, E. W. Hawkes, S. Follmer, *Sci. Robot.* **2020**, *5*, eaaz0492.
[3] E. W. Hawkes, L. H. Blumenschein, J. D. Greer, A. M. Okamura, *Sci. Robot.* **2017**, *2*, eaan3028.
[4] D. S. Shah, J. P. Powers, L. G. Tilton, S. Kriegman, J. Bongard, R. Kramer-Bottiglio, *Nat. Mach. Intell.* **2021**, *3*, 51.
[5] R. K. Katzschmann, J. DelPreto, R. MacCurdy, D. Rus, *Sci. Robot.* **2018**, *3*, eaar3449.
[6] W. Heng, G. Yang, G. Pang, Z. Ye, H. Lv, J. Du, G. Zhao, Z. Pang, *Adv. Intell. Syst.* **2021**, *3*, 2000038.
[7] M. Cianchetti, T. Ranzani, G. Gerboni, T. Nanayakkara, K. Althoefer, P. Dasgupta, A. Menciassi, *Soft Rob.* **2014**, *1*, 122.
[8] E. Acome, S. K. Mitchell, T. G. Morrissey, M. B. Emmett, C. Benjamin, M. King, M. Radakovitz, C. Keplinger, *Science* **2018**, *359*, 61.
[9] Z. Xing, J. Zhang, D. McCoul, Y. Cui, L. Sun, J. Zhao, *Soft Rob.* **2020**, *7*, 512.
[10] T. Li, G. Li, Y. Liang, T. Cheng, J. Dai, X. Yang, B. Liu, Z. Zeng, Z. Huang, Y. Luo, T. Xie, W. Yang, *Sci. Adv.* **2017**, *3*, 1602045.
[11] S. R. Goudu, I. C. Yasa, X. Hu, H. Ceylan, W. Hu, M. Sitti, *Adv. Funct. Mater.* **2020**, *30*, 2004975.
[12] E. B. Joyee, Y. Pan, *Soft Rob.* **2019**, *6*, 333.
[13] M. Manti, T. Hassan, G. Passetti, N. D'Elia, C. Laschi, M. Cianchetti, *Soft Rob.* **2015**, *2*, 107.
[14] V. Vikas, E. Cohen, R. Grassi, C. Sozer, B. Trimmer, *IEEE Trans. Robot.* **2016**, *32*, 949.
[15] H. In, B. B. Kang, M. K. Sin, K. J. Cho, *IEEE Robot. Autom. Mag.* **2015**, *22*, 97.
[16] E. Brown, N. Rodenberg, J. Amend, A. Mozeika, E. Steltz, M. R. Zakin, H. Lipson, H. M. Jaeger, *Proc. Natl. Acad. Sci. U. S. A.* **2010**, *107*, 18809.
[17] M. Runciman, A. Darzi, G. P. Mylonas, *Soft Rob.* **2019**, *6*, 423.
[18] P. Polygerinos, N. Correll, S. A. Morin, B. Mosadegh, C. D. Onal, K. Petersen, M. Cianchetti, M. T. Tolley, R. F. Shepherd, *Adv. Eng. Mater.* **2017**, *19*, 1700016.
[19] F. Ilievski, A. D. Mazzeo, R. F. Shepherd, X. Chen, G. M. Whitesides, *Angew. Chemie* **2011**, *123*, 1930.
[20] B. Mosadegh, P. Polygerinos, C. Keplinger, S. Wennstedt, R. F. Shepherd, U. Gupta, J. Shim, K. Bertoldi, C. J. Walsh, G. M. Whitesides, *Adv. Funct. Mater.* **2014**, *24*, 2163.
[21] Y. Tang, Y. Chi, J. Sun, T. H. Huang, O. H. Maghsoudi, A. Spence, J. Zhao, H. Su, J. Yin, *Sci. Adv.* **2020**, *6*, eaaz6912.
[22] H. K. Yap, H. Y. Ng, C. H. Yeow, *Soft Rob.* **2016**, *3*, 144.
[23] F. Connolly, P. Polygerinos, C. J. Walsh, K. Bertoldi, *Soft Rob.* **2015**, *2*, 26.
[24] D. Yang, M. S. Verma, E. Lossner, D. Stothers, G. M. Whitesides, *Adv. Mater. Technol.* **2017**, *2*, 1600164.
[25] S. Koizumi, S. Kurumaya, H. Nabae, G. Endo, K. Suzumori, *IEEE Robot. Autom. Lett.* **2018**, *3*, 3240.
[26] K. P. Becker, Y. Chen, R. J. Wood, *Adv. Funct. Mater.* **2020**, *30*, 1908919.
[27] J. Deiters, W. Kowalczyk, T. Seidl, *Biol. Open* **2016**, *5*, 638.
[28] K. Saito, S. Nomura, S. Yamamoto, R. Niyama, Y. Okabe, *Proc. Natl. Acad. Sci. U. S. A.* **2017**, *114*, 5624.
[29] S. M. Baek, S. Yim, S. H. Chae, D. Y. Lee, K. J. Cho, *Sci. Robot.* **2020**, *5*, eaaz6262.
[30] D.-Y. Lee, J.-K. Kim, C.-Y. Sohn, J.-M. Heo, K.-J. Cho, *Sci. Robot.* **2021**, *6*, eabe0201.
[31] Y. Lin, G. Yang, Y. Liang, C. Zhang, W. Wang, D. Qian, H. Yang, J. Zou, *Adv. Funct. Mater.* **2020**, *30*, 2000349.
[32] S. J. Kim, D. Y. Lee, G. P. Jung, K. J. Cho, *Sci. Robot.* **2018**, *3*, eaar2915.
[33] H. Suzuki, R. J. Wood, *Nat. Mach. Intell.* **2020**, *2*, 437.
[34] M. Schenk, A. D. Viquerat, K. A. Seffen, S. D. Guest, *J. Spacecr. Rockets* **2014**, *51*, 762.
[35] N. A. Pehrson, D. C. Ames, S. P. Smith, S. P. Magleby, M. Arya, *AIAA J.* **2020**, *58*, 3221.
[36] M. Johnson, Y. Chen, S. Hovet, S. Xu, B. Wood, H. Ren, J. Tokuda, Z. T. H. Tse, *Int. J. Comput. Assist. Radiol. Surg.* **2017**, *12*, 2023.
[37] R. V. Martinez, C. R. Fish, X. Chen, G. M. Whitesides, *Adv. Funct. Mater.* **2012**, *22*, 1376.
[38] S. Li, D. M. Vogt, D. Rus, R. J. Wood, *Proc. Natl. Acad. Sci. U. S. A.* **2017**, *114*, 13132.
[39] B. Chen, Z. Shao, Z. Xie, J. Liu, F. Pan, L. He, L. Zhang, Y. Zhang, X. Ling, F. Peng, W. Yun, L. Wen, **2021**, 2000251.
[40] J. A. Faber, A. F. Arrieta, A. R. Studart, *Science* **2018**, *359*, 1386.
[41] S. Mintchev, J. Shintake, D. Floreano, *Sci. Robot.* **2018**, *3*, eaau0275.
[42] W. Kim, J. Byun, J. K. Kim, W. Y. Choi, K. Jakobsen, J. Jakobsen, D. Y. Lee, K. J. Cho, *Sci. Robot.* **2019**, *4*, eaay3493.
[43] R. Niiyama, X. Sun, C. Sung, B. An, D. Rus, S. Kim, *Soft Rob.* **2015**, *2*, 59.
[44] T. Tachi, K. Miura, *J. Int. Assoc. Shell Spat. Struct.* **2012**, *53*, 217.
[45] *mGrip modular gripping system (Soft Robotics, inc.)*, https://www.softroboticsinc.com/products/mgrip-modular-gripping-solution-for-machine-builders, (accessed: May 2021).
[46] Z. Wang, Y. Torigoe, S. Hirai, *IEEE Robot. Autom. Lett.* **2017**, *2*, 1909.
[47] J. H. Low, J. Y. Goh, N. Cheng, P. M. Khin, Q. Q. Han, C. H. Yeow, in *2020 IEEE Int. Conf. Robot. Autom.*, IEEE, Piscataway, NJ **2020**, pp. 7979–7985.
[48] *The RightPick system (RightHand Robotics, Inc.)*, https://www.righthandrobotics.com/products, (accessed: May 2021).
[49] A. Koivikko, V. Sariola, in *2019 IEEE Int. Conf. Soft Robot.*, IEEE, Piscataway, NJ **2019**, pp. 509–513.
[50] E. Sachyani Keneth, A. Kamyshny, M. Totaro, L. Beccai, S. Magdassi, *Adv. Mater.* **2021**, *33*, 1.
[51] T. J. Wallin, J. Pikul, R. F. Shepherd, *Nat. Rev. Mater.* **2018**, *3*, 84.


© 2021 The Authors. Advanced Intelligent Systems published by Wiley-VCH GmbH